Available online at www.sciencedirect.com
ScienceDirect
Journal of Catalysis 245 (2007) 338–347
JOURNAL OF CATALYSIS
www.elsevier.com/locate/jcat

Synergistic role of acid sites in the Ce-enhanced activity of mesoporous Ce–Al-MCM-41 catalysts in alkylation reactions: FTIR and TPD-ammonia studies

Pranjal Kalita, Narendra M. Gupta [1], Rajiv Kumar *

Catalysis Division, National Chemical Laboratory, Pune-411008, India

Received 27 June 2006; revised 24 October 2006; accepted 26 October 2006

Available online 28 November 2006

Abstract

The acidic properties of Ce_x–Al_y-MCM-41 with different Ce/Al/Si atomic ratios were examined by pyridine-FTIR and ammonia-TPD methods. Both the density and the strength of the acid sites were considerably higher in the samples containing both Ce and Al than in the samples with only one of these substituents. The IR spectra of chemisorbed pyridine revealed that the Ce–Al-MCM-41 samples contained at least two distinct Lewis acid sites, L_2 (1595–1444 cm^{-1}) and L_1 (1613–1452 cm^{-1}), where the L_2/L_1 ratio increased progressively with increasing Ce/Al atomic ratio in a series of samples with similar Si/Al ratios. In addition, the density of the Brönsted acid sites (B) as well as the B/L_1 ratio increased with increasing Ce/Al molar ratio in these samples. The findings of this study help us understand the synergistic role played by Lewis and Brönsted acid sites in the catalytic activity of these catalysts for the benzylation of toluene.

Keywords: Ce–Al-MCM-41; Ammonia-TPD; Pyridine-FTIR; Friedel–Crafts alkylation; Benzylation reaction

1. Introduction

Different synthesis strategies have been reported in the literature for incorporating acidic sites in otherwise chemically inert mesoporous silicate materials of the M41S family [1–4]. Substitutions of metal or nonmetal elements in the framework have by and large yielded fruitful results in these efforts, leading to improved catalytic properties of different silicate catalysts. For instance, it has been possible to generate significant catalytic activity in MCM-41 by incorporating divalent (Co, Zn), trivalent (Al, B, Fe, Cr), or tetravalent (Ti, V, Sn, Zr, Mn) metal ions in the structural network [3]. Nevertheless, few studies have been reported so far on isomorphous substitution of heterovalent lanthanides and the resultant catalytic properties of such mesoporous silicates. We have demonstrated that Ce-incorporated MCM-41 exhibited high activity for various catalytic reactions, such as acylation of alcohols, vapor-phase dehydrogenation of cyclohexanol to cyclohexane, hydroxylation of 1-naphthol with peroxides, and alkylation of naphthalene [5,6]. Similarly, Ce-incorporation in silica network of MCM-41 has been found to impart catalytic activity in the oxidation of cyclohexane [7] and *n*-heptane [8].

Although Ce-MCM-41 has been found to be a quite promising catalyst for Lewis acid-induced acylation reactions [6], H/Al-MCM-41 can catalyze both the Lewis acid- and Brönsted acid-catalyzed reactions due to its Lewis and Brönsted acidity. Furthermore, Ce–Al-MCM-41 samples, with simultaneous incorporation of Ce and Al in MCM-41, was found to exhibit higher catalytic activity for Brönsted acid-catalyzed isopropylation of naphthalene compared with Al-MCM-41 with comparable Al content [6]. How such dual incorporation of Ce and Al can enhance the Brönsted acidity as well as the total acidity of these Ce–Al-MCM-41 catalysts remains unexplored.

Consequently, we undertook pyridine-FTIR and ammonia-TPD studies on the H-form of calcined Ce-MCM-41, Al-MCM-41 and Ce–Al-MCM-41 samples with varying Ce/Al mol ratios. We also systematically monitored the effect of substitution on the O–H stretching bands of these materials. The overall objec-

* Corresponding author. Fax: +91 20 2590 2633.
E-mail address: r.kumar@ncl.res.in (R. Kumar).
[1] Emeritus scientist, CSIR.

0021-9517/$ – see front matter
doi:10.1016/j.jcat.2006.10.022

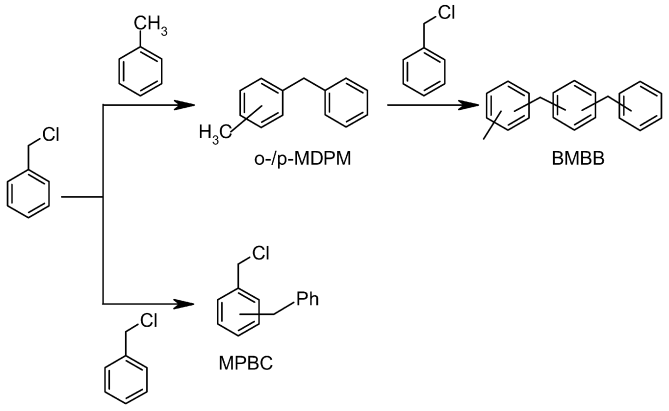

Scheme 1. Lewis acid-catalyzed benzylation of toluene using benzyl chloride.

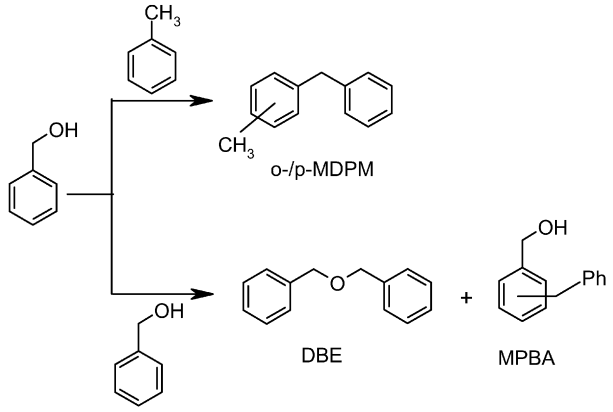

Scheme 2. Brönsted acid-catalyzed benzylation of toluene using benzyl alcohol.

tives of this study were to identify the acid sites generated in MCM-41 as a result of Ce and Ce + Al incorporation, and to explore the role of these sites in the Lewis acid- and Brönsted acid-catalyzed Friedel–Crafts alkylation reactions [9,10].

Considering the aforementioned issues, the benzylation of toluene with benzyl chloride and benzyl alcohol, the reactions catalyzed by Lewis acid and Brönsted acid sites, respectively [9,10], were chosen as the model catalytic reactions for this study. Schemes 1 and 2 depict the reaction products that form when benzyl chloride or benzyl alcohol is used as the alkylating agent, respectively. The main products in both cases were 1,4-methyldiphenylmethane (1,4-MDPM) and 1,2-methyldiphenylmethane (1,2-MDPM). However, for the Lewis acid-catalyzed route, small amounts of 1-benzyl-3-(4-methyl benzyl) benzene (BMBB) and methyl phenyl benzyl chloride (MPBC) were also obtained, whereas for Brönsted acid-catalyzed benzylation of toluene, the main side product was dibenzyl ether (DBE) along with minor amounts of methyl phenyl benzyl alcohol (MPBA) (see Schemes 1 and 2).

2. Experimental

2.1. Materials and synthesis

Fumed silica (Sigma–Aldrich, USA), NaOH (Merck, India), sodium aluminate ($NaAlO_2$, 42.0%, Al_2O_3, 39.0%, Na_2O and 19.0% H_2O; Loba Chemie, India), and Ce $(SO_4)_2{\cdot}4H_2O$ were used as raw materials. Cetyltrimethylammonium bromide (CTMABr; Loba Chemie, India) was used as a structure-directing agent.

The hydrothermal synthesis of Al-MCM-41, Ce-MCM-41, and Ce–Al-MCM-41 samples of various compositions was carried out in a Teflon-lined autoclave at 383 K for 24–36 h. The molar gel composition of various Ce-containing Al-MCM-41 samples was $1SiO_2{:}xCeO_2{:}yAl_2O_3{:}0.32NaOH{:}0.25CTMABr{:}125H_2O$, where $x = 0.013$–0.04 and $y = 0.02$–0.05.

After the hydrothermal treatment, the samples were washed thoroughly, first with distilled water and then with acetone, followed by drying at 353 K and calcinations at 773 K for 8 h in the presence of air. The calcined samples were treated twice with 0.5 M ammonium acetate solution (50 mL for a 1.0-g sample) and were then calcined again in air at 773 K for 7 h to finally obtain the H-form of different MCM-41 samples. All the samples were light-yellow in color. The samples were characterized using powder X-ray diffraction and physical adsorption of N_2 at 77 K. The elemental composition of calcined samples, determined by the atomic absorption method, is given in Table 1.

2.2. Alkylation reactions

The reactions were performed in batch mode and in liquid phase, using a glass reactor. Before the activity measurements, a catalyst sample (∼100 mg) was activated in air (423 K, 2 h) and then cooled to room temperature. Benzylation of toluene was carried out using two alkylating agents, benzyl chloride and benzyl alcohol. The substrate/alkylating agent molar ratio was ∼20:1.The progress of the reaction was followed for 6 h, by which time a complete conversion of the substrate was obtained in each experiment. The reaction mixture was centrifuged after cooling to room temperature. The separated organic layer was diluted with dichloromethane, and the product was analyzed using a Varian model-CP-3800 gas chromatograph equipped with a capillary column. The product identity was also confirmed by GC-MS.

2.3. IR studies

A Thermo Nicolet (model Nexus 870) FTIR equipped with a high-pressure high-temperature stainless steel cell, fitted with water-cooled CaF_2 windows, and described in detail previously [11], was used to record IR spectra in transmission mode. Self-supporting wafers (∼50 mg) of 25 mm diameter, placed in a sample holder block, were in direct contact with a chromel–alumel thermocouple. Samples were heated in situ for 8–10 h at 550–575 K under vacuum ($\sim 1 \times 10^{-3}$ Torr) to record the hydroxyl region bands and carry out pyridine adsorption experiments. For acidity measurements, samples were exposed at 420 K to multiple doses of pyridine (∼9.5 μmol each) until it reached saturation coverage. A gas mixture containing nitrogen gas saturated with pyridine vapor was used for this purpose. The gas pressure in the IR cell was monitored with the help of a digital capacitance manometer. IR spectra were plotted at

420 K after an equilibration time of 15–20 min for individual pulse injections. From these experiments, calibration data for each sample were obtained, indicating a relationship between the area under spectral lines corresponding to Lewis acid and Brönsted acid sites and the amount of pyridine adsorbed. Final spectra were recorded under two different temperature conditions to distinguish between the weak and strong adsorption sites: at 420 K, after 10 min, evacuation of the cell at the temperature of pyridine adsorption or, alternatively, at room temperature after postexposure cooling of the sample and subsequent evacuation. A total of 300 scans were co-added for plotting of each spectrum at a resolution of 4 cm^{-1}. The absorbance values of individual vibrational bands, shown in parentheses in some of the figures, were taken as a measure of the relative intensities for gross intercomparison.

2.4. Ammonia-TPD

Experiments on the saturation adsorption of ammonia and its subsequent temperature-programmed desorption (TPD-NH_3) were performed on a Micromeritics Autochem 2910 instrument. About 0.2 g of a fresh sample was placed in a U-shaped, flow-through, quartz microreactor for each experiment. The catalyst was activated at 775 K for 2 h under He flow (20 ml/min) and then cooled to 375 K before being exposed to ammonia. The sample was flushed again in He for 1 h to remove any physisorbed ammonia, and a desorption profile was then recorded by increasing the sample temperature from 375 to 773 K at a ramp rate of 5 K/min.

3. Results and discussion

3.1. Sample characteristics

All of the samples used in this study exhibited type IV isotherms, with hysteresis loops typical of mesoporous silicates. The Ce-substituted samples also exhibited a gradual decrease in BET surface area and a marginal increase in pore diameter. These morphological data are included in Table 1. Similarly, the powder XRD patterns of Si-MCM-41, Al-MCM-41, Ce-MCM-41, and Ce–Al-MCM-41 were similar to the reported hexagonal phase (p6mm) of MCM-41 samples, as shown in Fig. 1 for some representative compositions. The main (100) line, as well as (110), (200), and (210), reflections are clearly visible in these patterns. As a representative case, the XRD pattern of calcined Ce–Al-MCM-41 (sample F, with the highest Ce content) is shown in the inset of Fig. 1 to be in the range of 1.5°–60° (2°/min) along with the XRD patterns of physical mixture of 2.5% of CeO_2 in calcined Al-MCM-41 (sample A) and pure CeO_2. These data clearly show the absence of any secondary occluded free CeO_2 phase in the Ce-containing samples. These results are in agreement with our earlier reports on Ce-MCM-41 [5,6].

In contrast, a slight decrease in the peak intensities was observed in the Ce–Al-MCM-41 samples (Fig. 1d), indicating a marginal loss of crystalline character. Fig. 1d also shows a positive shift in the characteristic (100) reflection compared with that in the mesoporous Si-MCM-41 and Al-MCM-41 samples (Figs. 1a and 1b). This trend may be attributed to increased number of defect sites and certain bond strain in the Ce-containing samples. Some physicochemical properties of the catalysts are given in Table 1. The observed increase in unit cell parameter and pore diameter on incorporation of cerium in Al-MCM-41 (Table 1) suggests increased incorporation of the larger Ce^{4+} compared with Si^{4+} in the silicate framework. Here it must be mentioned that when we took the Si/Al ratio in the gel to be 20 (sample H), we could get Si/Al = 22 in the solid. However, the XRD pattern of this sample exhibited relatively very poor crystallinity/ordering and lower surface area (Table 1).

Table 1
Physicochemical characteristics of Al-MCM-41, Ce-MCM-41 and Ce–Al-MCM-41 samples

Sample	Catalysts[a]	Solid product		Ce/Al molar ratio	S_{BET} (m^2/g)	d_{100} (Å)	a_0[c] (Å)	Pore diameter (Å)
		Si/Ce[b]	Si/Al[b]					
A	Al-MCM-41 (–, 25)	0	30	–	1104	37.88	43.74	27.9
B	Ce-MCM-41 (75, –)	80	0	–	886	37.73	43.57	26.8
C	Ce-MCM-41 (25, –)	35	0	–	850	37.63	43.32	27.1
D	Ce–Al-MCM-41 (75, 25)	80	32	0.41	989	38.44	44.38	29.5
E	Ce–Al-MCM-41 (50, 25)	59	33	0.56	971	38.43	44.37	30.85
F	Ce–Al-MCM-41 (25, 25)	38	34	0.93	940	38.41	44.35	31.14
G	Al-MCM-41 (–, 50)	–	56	–	844	37.44	43.24	–
H	Al-MCM-41 (–, 20)	–	22	–	733	37.12	42.86	–

[a] First and second numbers in parentheses represent the Si/Ce and Si/Al mole ratio in gel, respectively.
[b] Solid product calculated by AAS.
[c] a_0, unit cell parameter $= 2d_{100}/\sqrt{3}$.

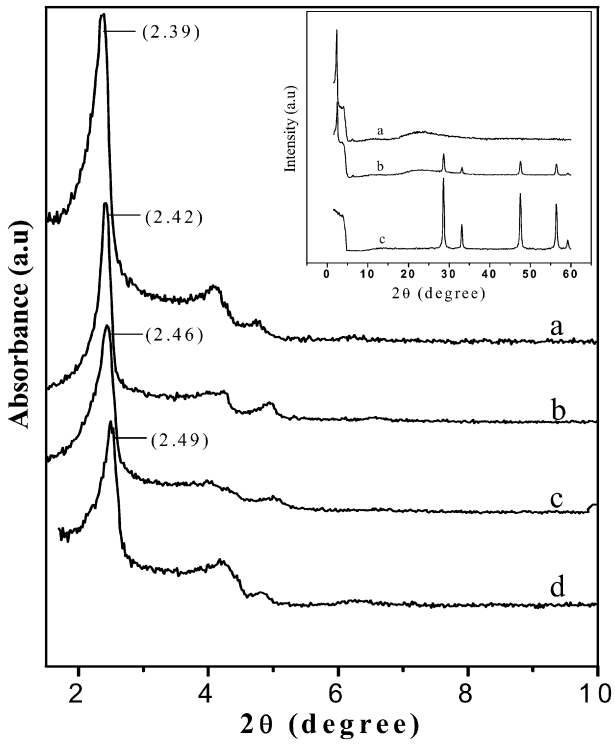

Fig. 1. Powder XRD patterns of (a) SiMCM-41, (b) AlMCM-41, (c) Ce-MCM-41 and (d) Ce–Al-MCM-41. Inset: XRD pattern of (a) Ce–Al-MCM-41 (sample F), (b) physical mixture of 2.5% of CeO_2 in Al-MCM-41 (sample A) and (c) Pure CeO_2.

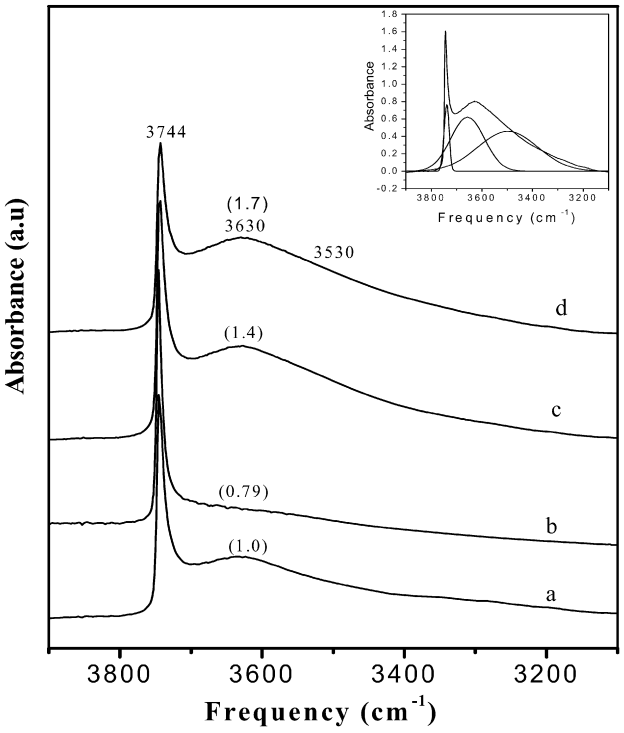

Fig. 2. Hydroxy region IR spectra of activated Ce–Al-MCM-41 samples containing similar Si/Al ratio (∼25) but different Ce content. The absorbance values of individual bands are given in parentheses, curve (a) sample A, no Ce; (b) sample C, no Al; (c) sample E, Ce/Al = 0.6; (d) sample F, Ce/Al = 0.9. Inset: deconvolution of ν(OH) bands in Fig. 2d.

3.2. Infrared spectroscopy study

3.2.1. O–H stretching bands

Fig. 2 presents the hydroxy region vibrational bands of Ce_x–Al_y-MCM-41 samples, containing similar Si/Al ratio (∼25) but different amounts of Ce, including a sample of Ce-MCM-41 in which no Al is present (Fig. 2, curve b). Corresponding data for the samples containing comparable Si/Ce ratios and increased amounts of Al are given in Fig. 3. As shown in Figs. 2 (curve b) and 3 (curve a), the samples containing Ce but no Al exhibited strong silanol groups (≡Si–OH, 3744 cm^{-1}), with negligible absorbance noted in the lower-frequency region. The presence of aluminum gave rise to a broad infrared band with a maximum at 3630 cm^{-1} (Fig. 2, curve a), with a full width at half maxima (FWHM) value of ∼140 cm^{-1}. Furthermore, a considerable increase in the intensity of this band was observed in the samples comprising both Ce and Al. In addition, a broad absorbance band at ca. 3530 cm^{-1} and tailing to the lower wavenumber side was also observed in the Ce–Al-MCM-41 samples (Fig. 2, curves c and d; Fig. 3, curves c and d). The presence of the low-frequency vibrational band at ca. 3530 cm^{-1} became apparent on deconvolution of the ν(OH) bands, as shown in the plot given in the inset of Fig. 2 as a typical case. A specific correlation between the intensity of different IR bands and the extent of heteroatom substitution in MCM-41 is also noticeable. Thus, in samples D–F containing comparable amounts of Al (Table 1), the intensity of the silanol band at 3744 cm^{-1} was found to decrease progressively, whereas that of the low-frequency region

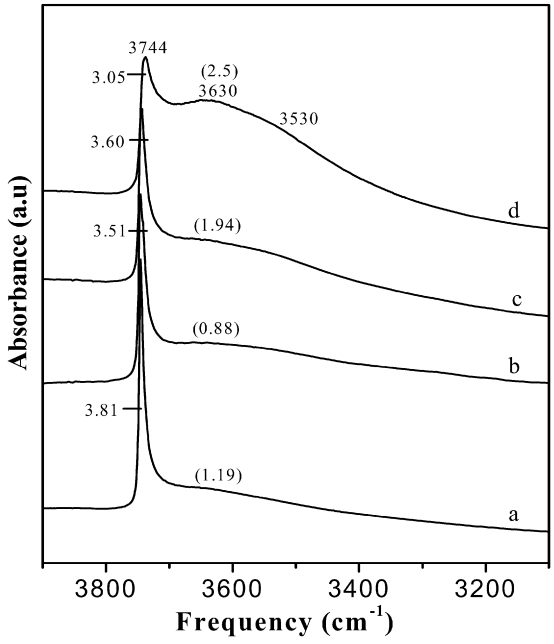

Fig. 3. Hydroxy region IR spectra of activated Ce–Al-MCM-41 samples containing similar Si/Ce atomic ratio (∼75) but different Al content. The absorbance values of individual bands are given in parentheses, curve (a) sample B, no Al; (b) sample D, Ce/Al = 0.4; (c) sample G, Ce/Al = 0.7; (d) sample I, Ce/Al = 1.3.

bands increased with increasing Ce/Al content (Fig. 2, curves a, c, and d); these data are plotted in Fig. 4. A similar trend is also noticeable in the IR spectra of Fig. 3. As expected, the intensity

of this band increased progressively with the increased amount of Al (Fig. 3) at comparable amounts of Ce. Furthermore, the overall acid site concentration, as estimated from the area under the ν(OH) region absorbance bands, increased progressively as a function of Ce/Al ratio.

The hydroxy region vibrational bands of MCM-41 have been reported widely; their frequency and concentration depend on various factors, including Si/Al ratio and the extent of dehydroxylation [12–14]. The 3744 cm^{-1} band arises due to isolated Si–OH groups. The band at 3660 cm^{-1}, observed for Al-MCM 41 but not in Si-MCM-41, is assigned to the hydroxy groups on coordinatively unsaturated aluminum oxide species that serve as Lewis acid sites. The lower-frequency band at ~3530 cm^{-1} was also reported earlier and was assigned to certain hydrogen-bonded silanol groups [13]. In the present study, we found that the intensity of lower-frequency region bands, particularly the one at 3530 cm^{-1}, increased considerably with increasing aluminum content and also with increasing Ce/Al atom ratio (Fig. 2, curves c and d; Fig. 3, curves c and d). We also found that the increased intensity of these bands was normally accompanied by a decreased concentration of silanol groups (3744 cm^{-1} band) (Fig. 4).

The pyridine adsorption results, discussed later, also showed that the concentration of Brönsted acid sites and certain Lewis acid sites increased considerably as a result of Ce incorporation in Al-MCM-41. Thus, the 3630 cm^{-1} band can be assigned to bridge-bonded species, in agreement with the IR spectral features of microporous zeolites such as H/ZSM-5, FAU, and BEA, where the O–H stretching band at ~3650 cm^{-1} is identified with the Al–(OH)–Si– type species [15]. A recent IR study by Gora-Marek and Datka [16] attributed a similar low-frequency band in H/MCM-41 and H/MCM-48 aluminosilicates to Si–(OH)–Al groups, giving rise to the Brönsted acidity in these mesoporous materials. The band at ~3530 cm^{-1}, with a negative shift of ~200 cm^{-1} with respect to the vibrational band of the silanol group, represents weak bonding and may arise due to hydroxyl groups associated with isolated cerium sites (Figs. 2 and 3, curve d).

3.2.2. Pyridine adsorption

Fig. 5 presents IR spectra of Al-MCM-41 (sample A, 3.2 at% Al), recorded at 420 K after exposure at this temperature to four consecutive pulses of pyridine vapor (9.5 μmol each). For a lower pyridine coverage (curve a), we observe mainly a pair of bands at 1613 and 1452 cm^{-1}, arising due to 8a ν(C–C) and 19b ν(C–C) vibrations of pyridine adsorbed at Lewis acid (designated as L_1) sites. Another pair of bands can be seen at 1636 and 1545 cm^{-1} due to the vibrations of pyridine molecules bound at bridge-bonded Brönsted (B) sites. Yet another intense band in this spectrum at 1490 cm^{-1} arose due to contributions of both the Lewis acid and Brönsted acid sites to pyridine adsorption. With increasing pyridine loading, a new pair of bands can be observed at 1595 and 1444 cm^{-1} (referred to as L_2 sites), whereas the intensity of the other bands mentioned above also increased progressively, with the B/L_1 ratio remaining almost the same (Fig. 5, curves b–d). Cooling of the sample to ambient temperature (~300 K) resulted in a pronounced increase intensity of the bands at 1595 and 1444 cm^{-1}, whereas the intensity of the other bands changed only marginally. Similarly, the intensity of the L_2 bands decreased to a greater extent on subsequent evacuation of the IR cell, as compared to the intensity of all other bands mentioned above. Fig. 6 exhibits comparative IR spectra of different samples, recorded at 300 K after saturation adsorption of pyridine

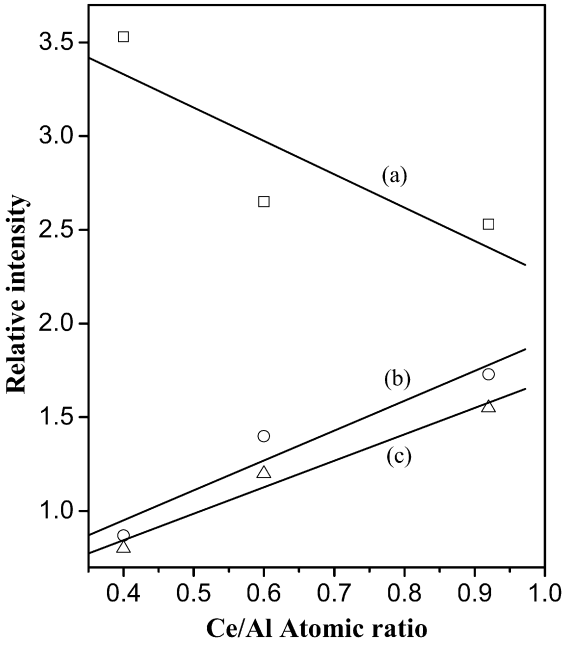

Fig. 4. Variation of intensity (absorbance) of different O–H stretching bands in Fig. 1, as a function of increasing Ce/Al ratio in Ce–Al-MCM-41 samples, curve (a) 3744, (b) 3630, and (c) 3520 cm^{-1}.

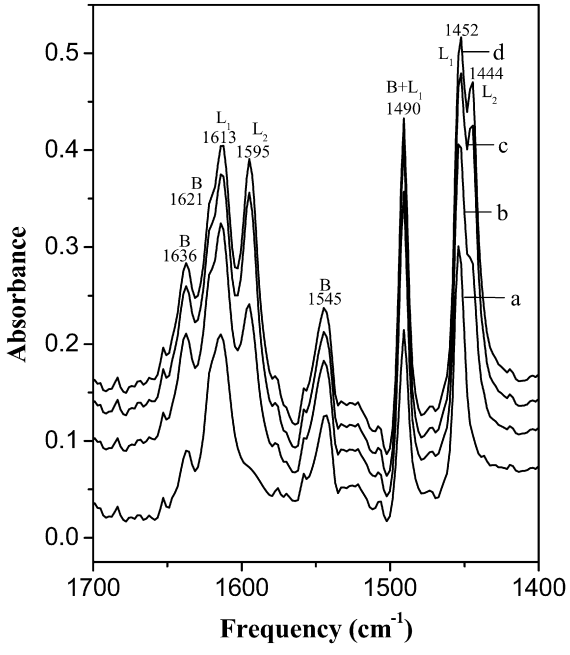

Fig. 5. IR spectra of Al-MCM-41 (Si/Al = 25, sample A), exposed to different doses of pyridine at 420 K, curve (a) 9.5, (b) 19.0, (c) 28.5, and (d) 38.0 μmol g^{-1}.

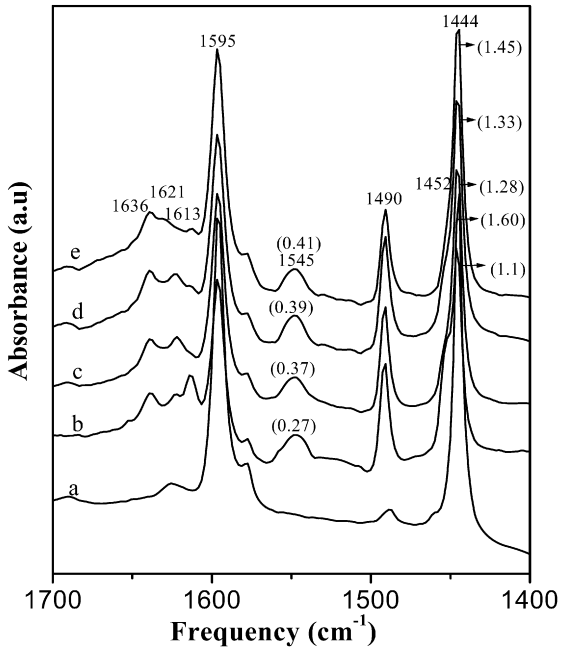

Fig. 6. IR spectra of Ce–Al-MCM-41 samples, recorded at 300 K after exposure to saturation coverage of pyridine at 420 K followed by cooling to room temperature and subsequent evacuation. Curve (a) sample C, Ce-MCM-41; (b) sample A, Al-MCM-41; (c) sample D, Ce/Al = 0.4; (d) sample E, Ce/Al = 0.6; (e) sample F, Ce/Al = 0.9.

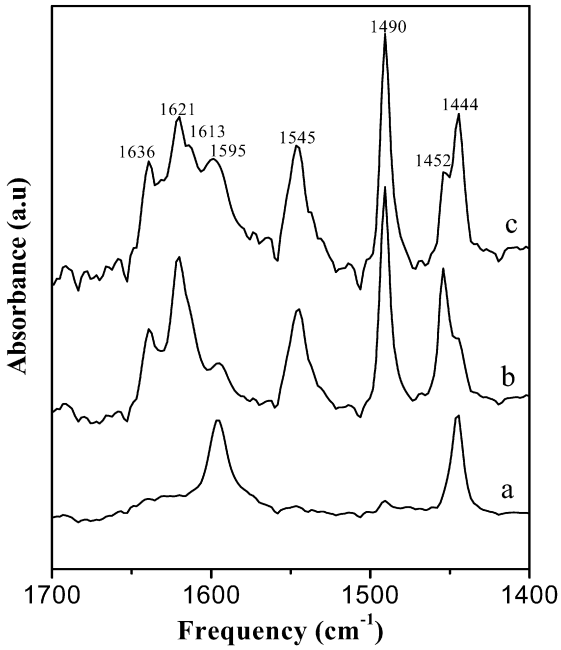

Fig. 7. IR spectra of Ce–Al-MCM-41 samples, recorded at 420 K after exposure to saturation coverage of pyridine at 420 K followed by evacuation for 10 min at same temperature. Curve (a) Ce-MCM-41, sample C; (b) Al-MCM-41, sample A and (c) Ce–Al-MCM-41, sample E, Ce/Al = 0.6.

at 420 K followed by cooling to ambient temperature and subsequent pumping for 10–15 min. These results reveal that the relative intensity of IR bands is influenced differently when Ce alone or Ce + Al were substituted in a sample. In the case of Ce-MCM-41 (curve a), we observe mainly a pair of strong bands at 1595 and 1444 cm^{-1}, while the intensity of the other bands due to adsorption of pyridine at above-mentioned L_1 and B sites was very small as compared to Al-MCM-41 (spectrum b). In the case of samples having co-substituted Ce and Al (curves c–e), an important change to be noticed is a progressive increase in the intensity of the Brönsted site IR bands (1545, 1621 and 1636 cm^{-1}), as reflected in the absorbance values marked on these spectra. A progressive increase is also noticeable in the intensity of the 1444 and 1595 cm^{-1} bands as a function of increasing Ce content.

Furthermore, the relative intensity of above-mentioned IR bands changed considerably when the samples exposed to saturation coverage of pyridine were evacuated at 420 K instead of at room temperature. Fig. 7 presents such representative spectra recorded at 420 K. An important feature of these results is a considerable decrease in the relative intensity of L_2 bands compared with that shown in Fig. 6. The concentration of the individual acid sites in different Ce–Al-MCM samples, calculated from the area under corresponding lines and using calibration values as mentioned in Section 2, along with the changes in their relative concentrations as a function of Ce and Al content are given in Table 2 for comparison. Also note that the ratio of L_2/L_1 further decreased when the sample temperature was raised above 425 K, indicating weak binding of pyridine at L_2 acid sites.

The IR bands appearing at 1595 and 1444 cm^{-1} (L_2) in Figs. 5–7 have been attributed to different types of adsorption sites, including hydrogen-bonded pyridine, because of the closeness of their frequency to that of the uncoordinated pyridine [14–17], and to certain weak Lewis acid sites, based on the fact that a similar pair of bands has been reported for the adsorption of pyridine over materials exhibiting strong Lewis acid character, such as zeolites, metal oxides, and clays [10,18]. In the present study, these bands were reasonably stable under evacuation at 420 K (Fig. 7), a trend not expected from hydrogen-bonded pyridine. At the same time, the intensity of these bands decreased considerably with increasing temperature (Table 2), indicating the weak bonding of pyridine at these sites. A similar pair of strong bands was observed in our earlier study on the adsorption of pyridine over titania, which exhibited high catalytic activity for Lewis acid-catalyzed orthoselective methylation of phenol [19]. In view of these observations, the pair of bands at 1595 and 1444 cm^{-1} (L_2 sites) may be attributed to certain weak Lewis acid sites. Based on the ratio of L_2/L_1 sites in different samples (Table 2), it can be concluded that the L_2 adsorption sites are promoted by the presence of Ce in a sample. These results are in agreement with the spectral features in Figs. 2 and 3. Our interpretation finds support in the study of Yiu and Brown [10] that found a similar pair of distinct Lewis acid sites in adsorption of pyridine over cation-exchanged mesoporous solid acid catalysts.

In conclusion, the data on acid site distribution given in Table 2 clearly reveal that the presence of Ce in Ce–Al-MCM-41 samples resulted in increased concentration of Brönsted acid sites and in the overall acid site concentration in these samples. Also, the substitution of Ce promoted the development of certain L_2 Lewis sites with weak pyridine binding compared with

Table 2
Concentration of Brönsted (B) and Lewis (L_1, L_2) sites and total acidity in Ce–Al-MCM-41 catalysts

Sample	Catalysts	Ce/Al mole ratio	Acid site concentration (μmol pyridine g^{-1})[a]				At 420 K[b]		At 300 K[b]		Total acidity[c] (μmol NH_3 g^{-1})
			L_2 (1444 cm^{-1})	L_1 (1454 cm^{-1})	B (1545 cm^{-1})	Total	L_2/L_1	B/L_1	L_2/L_1	B/L_1	
C	Ce-MCM-41 (25, 0)	–	169.7	40.0	0.0	209.7	4.2	0.0	13.7	0.0	160.6
A	Al-MCM-41 (0, 25)	–	62.4	140.2	120.0	322.6	0.4	0.8	1.6	0.4	334.5
D	Ce–Al-MCM-41 (75, 25)	0.4	58.6	101.1	190.0	349.7	0.6	1.9	2.3	0.6	365.7
E	Ce–Al-MCM-41 (50, 25)	0.6	120.3	110	154.0	384.3	1.1	1.5	2.5	0.7	419.7
F	Ce–Al-MCM-41 (25, 25)	0.9	140.0	115	207.0	462.0	1.2	1.8	3.5	1.1	468.3
G	Al-MCM-41 (0, 50)	–	–	–	–	–	–	–	–	–	325.2
H	Al-MCM-41 (0, 20)	–	–	–	–	–	–	–	–	–	300.2

[a] Spectra recorded at 420 K, on samples exposed to pyridine and then evacuated at same temperature.
[b] Spectra recorded at 300 K, on samples exposed to pyridine at 420 K followed by cooling to room temperature and subsequence evacuation.
[c] Measured by using TPD-NH_3 method.

that in Lewis sites associated with Al cations. Furthermore, the higher acidity of Ce–Al-MCM samples compared with that of Ce-MCM-41 or Al-MCM-41 (Table 2) provides clear evidence of a kind of synergism that may exist between the Al and Ce cations in the dual-substituted samples. The higher B/L_1 ratios in the data collected at 420 K (Table 2) indicate a greater binding strength of Brönsted acid site-bound pyridine, which may in turn influence the overall acid strength of dual-substituted samples, as was observed in the NH_3-TPD results described below.

3.3. TPD of ammonia

The ammonia-TPD profiles of the catalysts with different ratios of Si/Al and Si/Ce are shown in Fig. 8. As can be seen in this figure, all of the samples show a broad desorption signal in the region of 400–600 K, indicating a wide distribution of the surface acid strength. The total amount of ammonia desorbed is listed in Table 2, and the data are plotted in the inset of Fig. 8 as a function of Ce/Al ratio in different samples. These data reveal that compared with individual acidity of Al-MCM-41 and Ce-MCM-41, the overall concentration of acid sites was higher in Ce–Al-MCM-41, and it varied almost linearly as a function of Ce content. The ammonia-TPD data are thus in accordance with our IR results described above and confirm the Ce-induced enhancement of total acidity in the Ce–Al-MCM samples. Besides the increased concentration of acid sites, Fig. 8 also shows a progressive increase in TPD peak maximum by ∼20 K. These results are indicative of overall increase not only in the acid site concentration, but also in the strength of these sites as a result of Ce incorporation. However, the total acidity values of Al-MCM-41 samples A (Si/Al = 30), G (Si/Al = 56), and H (Si/Al = 22) were found to be 334.5, 325.2, 300.2 μmol NH_3, respectively, passing through a maxima for sample A.

The probable sites responsible for enhancing the strength of acid sites in Ce–Al-MCM-41 samples vis-à-vis Al-MCM-41 at comparable Si/Al ratio can be represented as ≡Ce–(OH)–Al≡ and/or ≡Si–(OH)–Al≡$(O)_3$≡Si–O–Ce≡ species. Because Ce^{4+} has more electropositive character than Si^{4+}, the presence of Ce^{4+} in the direct vicinity of Al (≡Ce–(OH)–Al≡) and/or (≡Si–(OH)–Al–Si–O–Ce≡) moiety will impart higher acid strength to the bridging OH group (Brönsted acid sites) through pulling electrons toward itself, thereby further polarizing the bridging O–H bond and leading to increased ease of deprotonation and thus higher acid strength. At the same time, the presence of Ce in the silica network is expected to impart Lewis acidity due to its ability to accept loan pair of electrons. It is thus important to recognize that the incorporation of cerium may promote both Lewis and Brönsted acidity, as revealed by our IR results as well (Figs. 7 and 8).

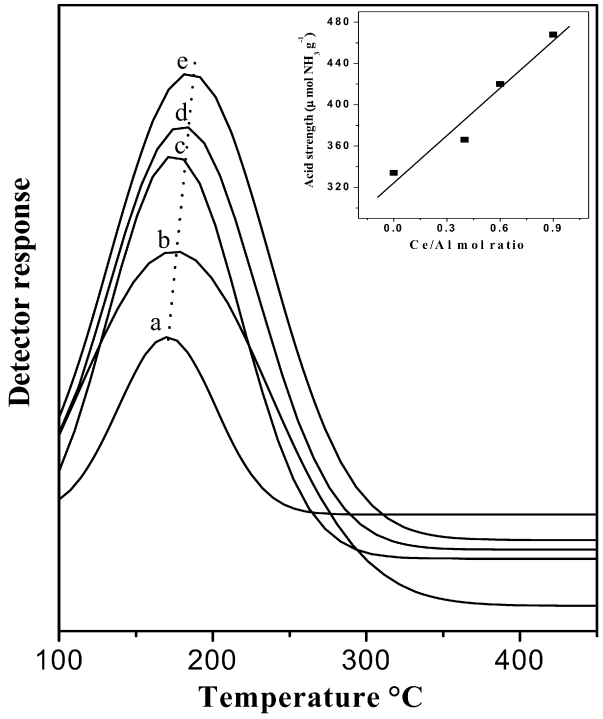

Fig. 8. Comparative TPD-NH_3 spectra of activated Ce–Al-MCM-41 samples as a function of composition. Inset plot: total acidity as a function of Ce/Al ratio in a sample. Curve (a) CeMCM-41; (b) AlMCM-41; (c) sample D, Ce/Al = 0.4; (d) sample E, Ce/Al = 0.6; (e) sample F, Ce/Al = 0.9.

3.4. Catalytic activity in Friedel–Crafts alkylation

Table 3 presents the data obtained for reaction of toluene and benzyl chloride over Ce_x–Al_y-MCM-41 samples at two different temperatures, where the main products are 1,2- and 1,4-MDPM. In addition, two other products formed by (i) further

benzylation of MDPM to 1-benzyl-3-(4-methyl benzyl) benzene (BMBB) and (ii) benzylation of benzylchloride to methyl phenyl benzyl chloride (MPBC) were also obtained (Scheme 1), particularly at lower temperature. The conversion was increased significantly by increasing the reaction temperature from 363 to 373 K (Table 3). The results given in this table also reveal that the Ce-MCM-41 (Si/Ce = 25) and Al-MCM-41 (Si/Al = 25) samples exhibit comparable catalytic activity at both the reaction temperatures, confirming that the incorporation of Ce in MCM-41 gave rise to a significant number of Lewis acid sites (L_2). It is of further interest to note that the presence of both Ce and Al resulted in significant increase in substrate conversion, the extent of which increased with increasing Ce/Al mol ratio at comparable Al contents. At the same time, a progressive increase in the yield of MDPM as a function of increasing Ce content with a consequent decrease in the yield of BMBB and MPBC were also observed. However, the selectivity for *o*- and *p*-isomers of the main reaction product remained unaffected by the Ce content at both reaction temperatures (Table 3).

Table 4 summarizes the results obtained using benzyl alcohol via the Brönsted acid-catalyzed route. As expected in light of the aforementioned FTIR results (Table 2), the Ce-MCM-41 sample exhibited no activity for Brönsted site-catalyzed alkylation of toluene using benzyl alcohol. In contrast, Al-MCM-41 showed very high activity, giving rise to methyldiphenylmethane (MDPM) as a major product. As in the case of benzyl chloride, here also two side products—methyl phenyl benzyl alcohol (MPBA) formed by the benzylation of benzyl alcohol and dibenzyl ether (DBE) formed by etherification via self-condensation of benzyl alcohol, as shown in Scheme 2—were also obtained. The rise in reaction temperature from 363 to 373 K resulted in increased conversion even though the selectivity for MDPM remained almost the same. However, as in the case of the data given in Table 3, the incorporation of Ce along with Al resulted in increased conversion of the substrate

Table 3
Liquid-phase alkylation of toluene with benzyl chloride at two reactions temperatures

Sample	Catalysts	Temp. (K)	BC conv. (mole%)	Product selectivity (%)[a]			
				o-MDPM	*p*-MDPM	BMBB	MPBC
C	Ce-MCM-41	363	42	37	38	13	12
	(25, –)	373	68	44	48	8	0
G	Al-MCM-41	363	33	34	35	15	16
	(–, 50)	373	60	41	42	14	3
A	Al-MCM-41	363	39	34	38	12	16
	(–, 25)	373	64	45	47	8	0
H	Al-MCM-41	363	35	32	36	14	18
	(–, 20)	373	58	43	42	10	3
D	Ce–Al-MCM-41	363	53	38	44	8	10
	(75, 25)	373	75	45	49	6	0
E	Ce–Al-MCM-41	363	59	41	45	6	8
	(50, 25)	373	81	45	51	4	0
F	Ce–Al-MCM-41	363	60	41	45	9	5
	(25, 25)	373	83	48	50	2	0

Catalyst = 0.1 g; reaction time: 6 h; toluene: benzyl chloride (BC): 20: (1 mole/mole).
[a] MDPM = 1,4-methyldiphenylmethane; BMBB = 1-benzyl-3-(4-methyl benzyl) benzene; MPBC = methyl phenyl benzyl chloride.

Table 4
Liquid-phase alkylation of toluene with benzyl alcohol at two reactions temperatures

Sample	Catalysts	Temp. (K)	BA conv. (mole%)	Product selectivity (%)[a]			
				o-MDPM	*p*-MDPM	DBE	MPBA
C	Ce-MCM-41	373	0	0	0	0	0
	(25, –)	383	0	0	0	0	0
G	Al-MCM-41	373	21	33	35	24	8
	(–, 50)	383	59	35	38	21	6
A	Al-MCM-41	373	22	37	39	13	11
	(–, 25)	383	62	37	39	24	0
H	Al-MCM-41	373	21	32	34	24	10
	(–, 20)	383	56	34	35	25	6
D	Ce–Al-MCM-41	373	29	41	43	9	7
	(75, 25)	383	70	40	42	18	0
E	Ce–Al-MCM-41	373	32	44	45	7	4
	(50, 25)	383	76	40	42	18	0
F	Ce–Al-MCM-41	373	33	43	45	5	7
	(25, 25)	383	78	45	43	12	0

Catalyst: 0.1 g; reaction time: 6 h; toluene: benzyl alcohol (BA): 20: 1 (mole/mole).
[a] MDPM = 1,4-methyldiphenylmethane; DBE = dibenzyl ether; MPBA = methyl phenyl benzyl alcohol.

and also in the increased yield of MDPM (Table 4). A marginal increase in the selectivity for DBE as a result of rise in temperature is also shown in Table 4. However, comparing only Al-MCM-41 samples with varying Si/Al (samples A, G, and H; Tables 3 and 4) demonstrated that conversion of benzyl chloride and benzyl alcohol passed through a maxima for sample A, in accordance with the total acidity data. However, the difference in the activity for the Al-MCM-41 sample was rather marginal vis-à-vis Ce–Al-MCM-41 samples. These results clearly suggest a synergistic effect of the incorporation of Ce into Al-MCM-41 in enhancing acidity and consequently catalytic activity in both Lewis acid- and Brönsted acid-catalyzed reactions.

Although it is clear that the incorporation of Ce in silicate network results in the generation of Lewis acid sites due to the ability of Ce^{4+} to accept a loan pair of electrons, generating new Brönsted acid sites in Ce–Al-MCM-41 in addition to bridged Si–OH–Al sites is rather interesting. Although at comparable Al contents, higher strength of the Brönsted acid sites in Ce–Al-MCM-41 can be expected based on the explanation given earlier in the discussion of TPD-NH_3, the increased density of Brönsted acid sites is intriguing; these values are expected to remain comparable at comparable Al contents irrespective of Ce^{4+} incorporation, because the Brönsted acidity is expected to be generated around Al^{3+} sites. Because Ce-MCM-41 and Ce–Al-MCM-41 samples were found to be ESR inactive, ruling out the presence of Ce^{3+} [5,6], the generation of new Brönsted acid sites in Ce–Al-MCM-41 merits careful investigation. It may be recalled (Fig. 2 and corresponding discussion) that the relative intensity of the free silanol band at 3744 cm^{-1} decreased progressively with increasing amounts of Ce at comparable Al contents in Ce–Al-MCM-41 samples and, consequently, the intensity of low-frequency region bands at 3530 cm^{-1} along with tailing to the lower wavenumber side increased with increasing Ce/Al content in a sample (Fig. 2, curves a, c, and d; Fig. 4). These low-frequency bands can be attributed to weakly hydrogen-bonded OH groups [13,16].

Considering all of this experimental evidence, a model for new Brönsted acid sites generated when both Ce and Al are present in silicate network is presented in Scheme 3. It is plausible that the polarized ≡Ce–O–H bonds can impart additional Brönsted acid sites to Ce–Al-MCM-41 samples, due to hydrogen bonded neighboring ≡Si–OH in the vicinity of ≡Ce–(OH)–Al≡ (Scheme 3A) or ≡Si–(OH)–Al≡ (Scheme 3B) moieties.

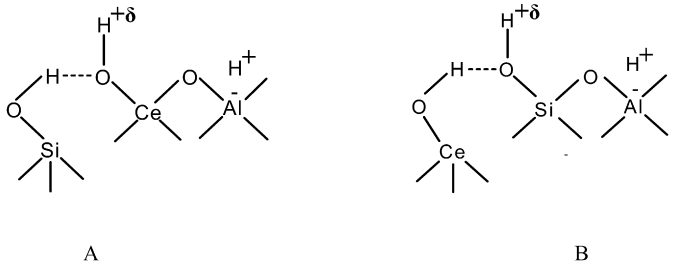

Scheme 3. Plausible new Brönsted acid sites generated due to simultaneous incorporation of Ce and Al in Ce–Al-MCM-41 samples.

It is pertinent to emphasize that no enhancement was observed in the catalytic activity of Ce-exchanged or Ce-impregnated Al-MCM-41 vis-à-vis H/Al-MCM-41, in either Lewis acid- or Brönsted acid-catalyzed reactions, in accordance with earlier results [6]. Thus, the Ce-induced enhancement of catalytic activity cannot be attributed to the presence of extra-network Ce^{4+} species either at the exchange site or possibly existing as occluded CeO_2 moieties.

4. Conclusion

The results of the present study point to a synergism between Ce and Al cations when co-substituted in siliceous MCM-41 during hydrothermal synthesis, resulting in a considerable increase in the concentration of both Lewis acid and Brönsted acid sites compared with Al-MCM-41 and Ce-MCM-41 samples. The IR spectra of chemisorbed pyridine reveal that the dual-substituted samples contained at least two distinct Lewis acid sites, designated as L_2 and L_1, with the L_2/L_1 ratio increasing progressively with the Ce/Al atom ratio. The sites L_1, found in abundance in Al-MCM-41, are identified with the conventional Lewis acid sites related to the presence of Al^{3+} at defect sites. The L_2 sites, associated with weakly bound pyridine, are identified with the isolated Ce species in silicate network. The decreased intensity of the silanol groups (Si–OH) and the consequent increase in the concentration of Brönsted acid sites on Ce incorporation provide an evidence for creation of new Brönsted acid sites as hydrogen-bonded polarized ≡Ce–OH or ≡Si–OH bonds in the vicinity of regular Brönsted acid sites (bridged OH moieties). The ammonia TPD results (Fig. 8) indicate that both the concentration and strength of the Brönsted acid sites increase as a result of Ce substitution. This may be attributed to the presence of more electropositive character of Ce^{4+} vis-à-vis Si^{4+} in the vicinity of Al^{3+}. The overall acidic character of the Ce–Al-MCM-41 samples is in complete harmony with the catalytic activity data, where the presence of Ce enhances catalytic activity for both the Lewis- and Brönsted-promoted benzylation reactions.

Acknowledgments

The authors thank Dr. S.P. Mirajkar, Dr. Nalini Jacob, and S. Violet for their kind cooperation with the TPD-NH_3, surface area, and XRD analyses, respectively. P.K. and N.M.G. thank CSIR, New Delhi, for a research fellowship grant and financial assistance through their Emeritus Scientist program, respectively.

References

[1] A. Corma, Chem. Rev. 97 (1997) 2373.
[2] X.S. Zhao, G.Q. (Max) Lu, G. Miller, Ind. Eng. Chem. Res. 35 (1996) 2090.
[3] S. Biz, M.L. Occelli, Cat. Rev. Sci. Eng. 41 (1998) 329.
[4] D. Trong On, D. Desplanier-Giscard, C. Danumah, S. Kaliaguine, Appl. Catal. A 253 (2003) 545.
[5] S.C. Laha, P. Mukharjee, S.R. Sainkar, R. Kumar, J. Catal. 207 (2002) 213.
[6] M.D. Kadgaonkar, S.C. Laha, R.K. Pandey, P. Kumar, S.P. Mirajkar, R. Kumar, Catal. Today 97 (2004) 225.

[7] W. Yao, Y. Chen, L. Min, H. Fang, Z. Yan, H. Wang, J. Wang, J. Mol. Catal. A Chem. 246 (2005) 161.
[8] S. Araujo, J.M.F.B. Aquino, M.J.B. Souza, A.O.S. Silva, J. Solid State Chem. 171 (2003) 371.
[9] G.A. Olah, Friedel–Crafts Chemistry, Wiley, New York, 1973.
[10] H.H.P. Yiu, D.R. Brown, Catal. Lett. 56 (1998) 57.
[11] N.M. Gupta, in: B. Viswanathan, S. Sivasanker, A.V. Ramaswamy (Eds.), Catalysis: Principles and Applications, Narosa, New Delhi, 2002, p. 127.
[12] A. Jentys, N.H. Pham, H. Vinek, J. Chem. Soc. Faraday Trans. 92 (1996) 3287.
[13] J. Chem, Q. Li, R. Xu, F. Xiao, Angew. Chem. Int. Ed. 34 (1995) 2694.
[14] S. Kawi, S.C. Shen, P.L. Chew, J. Mater. Chem. 12 (2002) 1582.
[15] A. Corma, Chem. Rev. 95 (1995) 559.
[16] K. Gora-Marek, J. Datka, Appl. Catal. A 302 (2006) 104.
[17] M. Selvaraj, B.R. Min, Y.G. Shul, T.G. Lee, Micropor. Mesopor. Mater. 74 (2004) 143.
[18] A.R. Gandhe, J.B. Fernades, S. Varma, N.M. Gupta, J. Mol. Catal. A Chem. 238 (2005) 63.
[19] M. Ziolek, I. Nowak, J.C. Lavalley, Catal. Lett. 45 (1997) 259.